How to cite: *Angew. Chem. Int. Ed.* **2024**, *63*, e202408570
doi.org/10.1002/anie.202408570

Perovskite-like Materials

Perovskite-Like Liquid-Crystalline Materials Based on Polyfluorinated Imidazolium Cations

Anastasios Stergiou[+], Leonardo Leccioli[+], Davide Ricci, Matteo L. Zaffalon, Sergio Brovelli, Francesca Baldelli Bombelli, Giancarlo Terraneo, Pierangelo Metrangolo, and Gabriella Cavallo**

Abstract: Hybrid Organic-Inorganic Halide Perovskites (HOIHPs) represent an emerging class of semiconducting materials, widely employed in a variety of optoelectronic applications. Despite their skyrocket growth in the last decade, a detailed understanding on their structure–property relationships is still missing. In this communication, we report two unprecedented perovskite-like materials based on polyfluorinated imidazolium cations. The two materials show thermotropic liquid crystalline behavior resulting in the emergence of stable mesophases. The manifold intermolecular F···F interactions are shown to be meaningful for the stabilization of both the solid- and liquid-crystalline orders of these perovskite-like materials. Moreover, the structure of the incorporated imidazolium cation was found to tune the properties of the liquid crystalline phase. Collectively, these results may pave the way for the design of a new class of halide perovskite-based soft materials.

Hybrid Organic-Inorganic Halide Perovskites (HOIHPs) are crystalline semiconductors that are reshaping the field of optoelectronic and photonic materials owing to their outstanding optical properties, such as tunable band gap, high photoluminescence quantum yield (PLQY), and facile solution processability, among others.[1] These unique features make them very promising candidates for high-end applications, e.g., solar cells (i.e., perovskite solar cells, PSCs),[2] light-emitting diodes,[3] photodetectors,[4] and field-effect transistors.[5] However, improving the control over crystallization of the perovskite layer and protecting it from atmosphere (i.e., oxygen, humidity) still remain unsolved issues to enable widespread adoption of these materials.[6]

Among the developed strategies to overcome these issues,[7] combining HOIHPs with liquid crystals and ionic liquids (ILs) has resulted in improving internal perovskite crystal integrity, passivating surface structural defects, blocking non-radiative recombination of photogenerated ion pairs, and preventing atmospheric-induced degradation,[8] thus promoting a remarkable advance of the recent research on IL-based PSCs.[9] The most explored ILs in PSCs are based on imidazolium (Im) salts, which have either been used as additives in the perovskite precursor solution[10] or as interfacial modifiers.[11] On one hand, it was found that the Im cation contributed as A-site cation, being also able to modify the dimensionality of the exposed perovskite surface.[11o] On the other hand, the Im counterion plays a multifunctional role ranging from halide source (Br^-, I^-), to hydrophobic shielding (BF_4^-, PF_6^-) of the perovskite/charge transport interface. Nevertheless, despite the improved efficiency and stability demonstrated by intensive studies and numerous reviews, a full understanding of the chemistry behind IL-based perovskites is still missing.[12]

To the best of our knowledge, all reported HOIHPs are crystalline solids. However, to fully realize the potential of this class of powerful semiconductors, we targeted to obtain the first examples of liquid crystalline (LC) HOIHPs, which may pave the way to novel functional soft materials[13] and expand the scope of metal-containing liquid crystals.[14] Herein, we present an unprecedented strategy for obtaining intrinsically LC HOIHPs, in which the liquid crystallinity is enabled by the use of Im-based fluorinated ionic liquid crystals (FILCs) as source of A-site cations.

Fluorination represents a powerful tool to control the self-assembly behavior of nanostructured materials via the *fluorophobic effect*,[15] namely the segregation of perfluorocarbon chains driven by fluorine-fluorine interactions.[15] In particular, for Im-based ILs, the introduction of polyfluorinated chains on the imidazolium core may promote the emergence of lamellar mesophases with beneficial effect on

[*] Dr. A. Stergiou,[+] L. Leccioli,[+] D. Ricci, Prof. Dr. F. B. Bombelli, Prof. Dr. G. Terraneo, Prof. Dr. P. Metrangolo, Prof. Dr. G. Cavallo
Laboratory of Supramolecular and Bio-Nanomaterials (SBNLab)
Department of Chemistry, Materials and Chemical Engineering "Giulio Natta"
Politecnico di Milano
Via L. Mancinelli 7, 20131 Milano (Italy)
E-mail: pierangelo.metrangolo@polimi.it
gabriella.cavallo@polimi.it

Dr. M. L. Zaffalon, Prof. Dr. S. Brovelli
Dipartimento di Scienza dei Materiali
Università degli Studi di Milano-Bicocca
Via R. Cozzi 55, 20125 Milano (Italy)

[+] These authors equally contributed to this work and share first authorship.

charge mobility. Such FILCs are, in fact, in the spotlight as quasi-solid state electrolytes in dye-sensitized solar cells (DSSCs).[16] Currently, there is only a couple of reports dealing with interactions of perovskites with ionic liquid crystals (ILCs), more specifically a side-chain liquid crystalline polymer[17] and a 4-cyanobiphenyl-terminated alkylammonium salt[18] used as additives in PSCs, with no account on the resulting LC properties. In this communication, we report two new HOIHPs obtained by reacting lead iodide (PbI_2) with thermotropic FILCs ($MeImC_{m+6}H_{2m}F_{13}I$, $m=$ 2,3), as illustrated in the Scheme 1.[15d]

Experimentally, we reacted PbI_2 and the $MeImC_{m+6}H_{2m}F_{13}I$ FILCs at different molar ratios (1:1, 1:2, 1:4) in boiling HI (57 %)/H_3PO_2 (50 %) mixture in water, followed by slow cooling (2 °C/h) to room temperature (see Experimental Procedures in the Supporting Information). In all ratios, thin yellowish crystal platelets (Figure S1) having all the same melting point (~140 °C) were obtained for $MeImC_9H_6F_{13}I$. Performing Fourier-transform infrared spectroscopy (FT-IR) on these isolated crystals derived from the different stoichiometries, no differences were observed between them. In all of the samples, the C=N and C=C imidazolium modes at ~1570 cm^{-1} were found to shift to lower wavenumbers, as compared to the pristine $MeImC_9H_6F_{13}I$, implying a different charge density on the aromatic core (Figure S2). This was further corroborated by examining the proton (^1H) and fluorine (^{19}F) nuclear magnetic resonance (NMR) spectra. In the ^1H NMR spectrum, strong shielding of the protons residing on the imidazolium core was evident (Figure S3a), while an analogous shielding trend was observed for the polyfluorinated chain (^{19}F NMR spectrum, Figure S3b). Further, mass spectrometry analyses (Figure S4) revealed the presence of PbI_3^-, $(MeImC_9H_6F_{13}I)I^-$, and $(MeImC_9H_6F_{13}I_2)I^-$ molecular ions in the negative mode, and the $(MeImC_9H_6F_{13})^+$ molecular ion in the positive mode, collectively indicating the fragmentation of a perovskite-like structure and the absence of lead oxide (PbO_x) species. Interestingly, the isolated yellowish crystals are environmentally stable, namely in open air at room temperature, for several months, and have a high thermal stability as demonstrated by thermogravimetric analysis (TGA). In detail, the onset temperature value for the first decomposition step, related to the gradual degradation of the organic part, was as high as 245 °C and the second weight loss step, originating from the decomposition of the inorganic part, had an onset at ~425 °C (Figure S5).

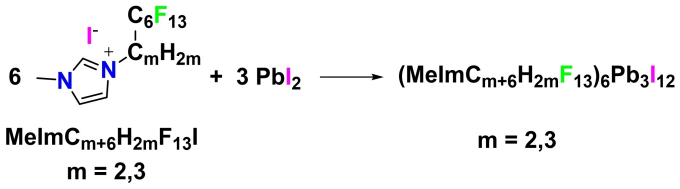

Scheme 1. Molecular formulae of the obtained fluorinated perovskite-like materials and starting compounds thereof.

The optical properties of the isolated crystals were studied by continuous wave (cw) and time-resolved spectroscopy. The optical absorption profile (Figure 1a, black line) featured a sharp transition at 3.34 eV with a shoulder at ~3 eV, Stokes-shifted by ~0.4 eV from a narrow emission (NE) peak at 2.43 eV and followed by a weak broad emission (BE) contribution at ~1.9 eV (Figure 1a, purple line). This behavior is intrinsic in low dimensional perovskites,[19] where the two emission contributions are ascribed to the decay of free excitons (NE) and the recombination of trapped excitons mediated by halide vacancies (BE). The PLE spectrum resembled well the absorption profile, indicating that the two emissions occurred from the same states irrespective of the excitation energy. Consistent with the low emission efficiency (PLQY < 1%), the room-temperature time dynamics of the NE was resolution limited (faster than 800 ps) and the decay of the BE featured an effective lifetime (estimated as the time after which the intensity decreased by a factor e) of $\tau_{EFF}=2$ ns indicating strong non-radiative quenching (vide *infra*).

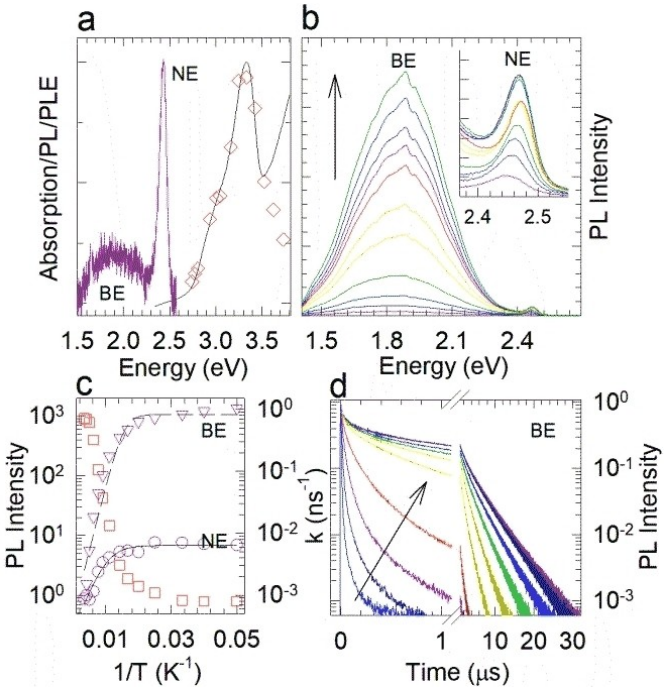

Figure 1. a) Optical absorption (black line), PL (purple line, excitation at 3.31 eV), and PLE (diamonds) spectra at room temperature. Both the absorption growth and PLE drop above 3.5 eV were due to large UV reflectance. b) PL spectra at decreasing temperature (as indicated by the arrow) from 300 K to 20 K. Inset: detail of the NE contribution. c) Spectrally integrated PL intensity as extracted from 'b' (normalized for the maximum value at 300 K, triangles for the BE and circles for the NE) and the corresponding BE decay rate (red squares) as extracted from 'd'. The dashed lines are the fitting curves to the Arrhenius equation: $I(T)=I_0/(1+A\exp(-E_a/k_BT))$, where I_0 is the ideal PL intensity at 0 K, A is a multiplying factor and E_a is the activation energy. d) BE decay curves at decreasing temperature (indicated by the arrow) from 300 to 20 K under 3.31 eV excitation.

Upon lowering the temperature, both emissions intensified without substantial shape or energy modifications, with a particularly strong growth of the BE that became largely dominant over the NE (Figure 1b). The intensity trends *vs.* T of the two luminescence contributions are quantified in Figure 1c. The best fit yielded $E_a = \sim 28$ meV and $E_a = \sim 43$ meV for the NE and BE respectively, indicating that thermal quenching was likely due to different phonon coupling for the two channels as commonly observed for free *vs.* localized excitons. Consistent with the large increase of BE emission intensity, the BE effective decay rate ($k_{EFF} = 1/\tau_{EFF}$) dropped dramatically with decreasing temperature from 0.5 ns^{-1} at 300 K to 5×10^{-4} ns^{-1} at 20 K, thus confirming that the weak room temperature BE was mostly due to multi-phonon non-radiative decay (Figure 1d). In turn, the NE lifetime remained essentially unchanged for the whole temperature range suggesting that free excitons are mostly quenched by barrierless carrier trapping, possibly in the structural defects also responsible for the BE which agrees with the monotonic growth of the BE emission. To summarize, regardless of the PbI_2:$MeImC_9H_6F_{13}I$ stoichiometry, all of the isolated crystals displayed the same optical properties, indicating a low-dimensional perovskite-like structure.

Single crystal X-ray diffraction analysis using synchrotron radiation revealed that all of the isolated crystals had the same chemical formula being $(MeImC_9H_6F_{13})_6Pb_3I_{12}$, regardless of the stoichiometry used for their syntheses (Table S1). Interestingly, the unit cell is composed by six asymmetric $MeImC_9H_6F_{13}^+$ cations and one trinuclear $Pb_3I_{12}^{6-}$ anionic cluster (Figure S6). Within the trinuclear cluster, each Pb^{2+} is hexacoordinated by 6 iodine atoms forming a distorted octahedral geometry. The 6 iodide anions surrounding the central Pb^{2+} cation adopt μ_2 connections linking the central Pb cation to the two adjacent ones and giving rise to a face-sharing connection of PbI_6 octahedra within the trinuclear cluster (Figure 2 and Figure S7). The Pb–I bond lengths are in the 3.079–3.371 Å range. The trinuclear $Pb_3I_{12}^{6-}$ cluster establishes an extended network of hydrogen bonds (HB) with the adjacent imidazolium cations, functioning as HB-acceptor for the hydrogen atoms of the imidazolium ring and the methylene groups of the polyfluorinated alkyl chain. The presence of several HB-donor fragments adjacent to the anionic cluster shield the $Pb_3I_{12}^{6-}$ unit, hampering the possible formation of more complex and extended architectures, such as 1D chains or 2D arrangements. As far as the polyfluoroalkyl chains are concerned, they are strongly affected by disorder (Figure S8). While the *N*-bound hydrocarbon segments adopt trans/gauche conformations in a 2:1 ratio, all of the fluorinated segments adopt the classical *all-trans* helical arrangement. Multiple F···F interactions occur between fluorinated chains of cations belonging to the same trinuclear $Pb_3I_{12}^{6-}$ anionic cluster (Figure S9). Finally, fluorinated chains of adjacent clusters partially interdigitate thanks to manifold F···F interactions and result in *fluorous* layers segregated from the cationic and anionic layers (Figure S10). This so-called *fluorophobic effect*[15c,e,20] promotes the crystallization of the layered hybrid fluoroorganic-organic–inorganic nanostructure (Figure 2). A comparison between the experimental powder X-ray diffraction pattern of the obtained crystalline materials and the one simulated from the single crystal proved the presence of only a single phase without impurities (Figure S11).

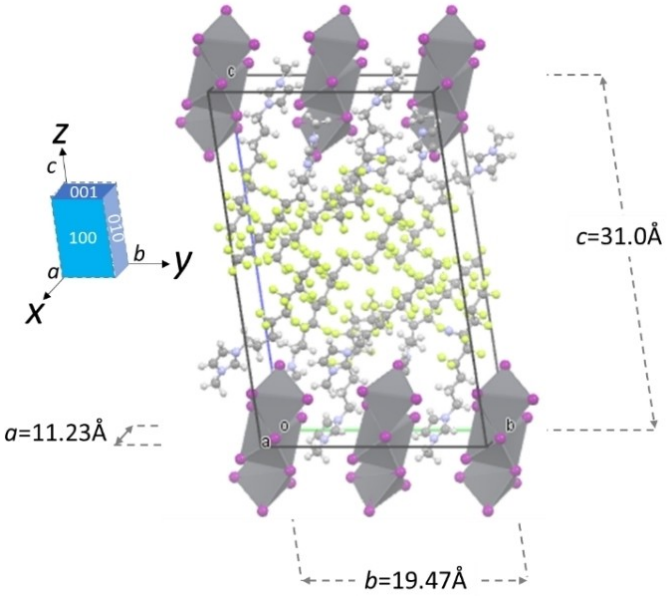

Figure 2. Representation of the crystal packing of $(MeImC_9H_6F_{13})_6Pb_3I_{12}$ accompanied by the length of *a*, *b*, and c crystallographic axes. Disorder of the perfluorinated segments and $Pb_3I_{12}^{6-}$ has been removed for clarity (See Table S1 and Figures S6–10 for further crystallographic details). Colour and style code: $Pb_3I_{12}^{6-}$, polyhedral representation; Pb, dark grey; I, purple; $MeImC_9H_6F_{13}^+$, ball and stick representation; C, grey; N, light blue; F, yellow; H, white.

Under the same synthetic route, we synthesized the second perovskite-like material starting from the $MeImC_8H_4F_{13}I$ FILC. The isolated yellowish platelets of $(MeImC_8H_4F_{13})_6Pb_3I_{12}$ were characterized by FT-IR (Figure S12), ^1H and ^{19}F NMR (Figure S13), mass spectrometry (Figure S14), and TGA (Figure S15). However, unfortunately, crystals were not of enough quality to get the high-resolution single-crystal structure, despite using synchrotron radiation. This second material has a lower melting point (~120 °C), implying the tunability of the thermal properties with the selected imidazolium cation.

The emerging liquid crystalline properties of the two new perovskite-like materials, $(MeImC_9H_6F_{13})_6Pb_3I_{12}$ and $(MeImC_8H_4F_{13})_6Pb_3I_{12}$, were exhaustively investigated by differential scanning calorimetry (DSC), polarized optical microscopy (POM), and small/wide-angle X-ray diffraction (SAXS-WAXS) analyses. Initially, we examined the thermal transitions of the parent FILCs (Table S2). $MeImC_9H_6F_{13}I$ has an enantiotropic crystal-to-Smectic A (Cr-SmA) transition at 83 °C followed by a SmA-to-isotropic state transition (SmA-Iso) at 197 °C (Figure S16a, 1st cycle).[15d] The same transitions for $MeImC_8H_4F_{13}I$ are 103 °C (Cr-SmA) and 217 °C (SmA-Iso), respectively (Figure S16b, 1st cycle). Both Cr-SmA transitions are preceded by order/disorder transitions at ~50 and ~100 °C, which disappear/

attenuate in the following cycles. On cooling from the isotropic phases, both FILCs show clear (Iso-SmA) transitions, and recrystallizations appear at lower temperatures, i.e., 45–50 °C. Figure S17 shows SmA POM textures of both FILCs.

Importantly, the two perovskite-like crystalline materials, $(MeImC_9H_6F_{13})_6Pb_3I_{12}$ and $(MeImC_8H_4F_{13})_6Pb_3I_{12}$, display Cr-SmA transitions, likewise the parent FILCs (Table S2). In detail, $(MeImC_9H_6F_{13})_6Pb_3I_{12}$ has a Cr-SmA transition at 144 °C, accompanied by a SmA-Iso transition at 241 °C (Figure 3a, Figure S16c). The SmA organization of the $(MeImC_9H_6F_{13})_6Pb_3I_{12}$ LC phase was validated by POM imaging (Figure 3b). Moving to the second perovskite-like material, $(MeImC_8H_4F_{13})_6Pb_3I_{12}$, the Cr-SmA transition occurs at 124 °C and clearing is reached at 251 °C (Figure 3c, Figure S16d). POM imaging of the LC phase also in this case confirmed the SmA texture (Figure 3d). Notably, the use of a higher melting point FILC resulted in a lower melting point perovskite-like material. Apart from the lower Cr-SmA transition, upon cooling the $(MeImC_8H_4F_{13})_6Pb_3I_{12}$ molten state, the LC phase underwent a slow vitrification, as revealed by POM imaging (Figure S18), as well as by DSC, where no recrystallization peak was ever observed (Figure S16d). Summarizing the POM and DSC studies, the two new perovskite-like materials, $(MeImC_9H_6F_{13})_6Pb_3I_{12}$ and $(MeImC_8H_4F_{13})_6Pb_3I_{12}$, were found to display unprecedented LC properties, stable for at least three consecutive heating/cooling cycles (Figures S16c-d, Table S2).

To shed more light on the observed Cr-SmA transitions and the organization of the mesophases, we studied their variable-temperature small and wide-angle X-ray (SAXS/WAXS) scattering profiles. Crystalline powders of $(MeImC_9H_6F_{13})_6Pb_3I_{12}$ show an ordered lamellar structure at room temperature with the primary SAXS peak as a strong and sharp reflection at $q = 0.20\ Å^{-1}$ (periodicity of ca. 31.4 Å) followed by a weaker 2nd-order reflection, similarly to the parent $MeImC_9H_6F_{13}I$ FILC (Figure S19a). Peaks above $0.5\ Å^{-1}$ are signatures of the high crystallinity of $(MeImC_9H_6F_{13})_6Pb_3I_{12}$. These peaks, in fact, disappear above the melting temperature (i.e., 150 °C), where the primary SAXS peak and its 2nd-order reflection are preserved, although shifted a little to $0.21\ Å^{-1}$ (periodicity of ca. 29.9 Å), which is consistent with the existence of a lamellar SmA phase.[21] These distances can be related to the short-range ordering in ILs, resulting from local separation of the polar (anion and cationic headgroups) and non-polar (perfluorinated chains) components (Figure 2) and is indicative of the presence of a bilayer structure with short-range order that accompanies the formation of a percolated structure.[22] Interestingly, this periodicity value matches well the length of the crystallographic *c* axis (001 plane) (Figure S20), which is associated to the spacing between the inorganic clusters (Figure 2 and Figure S7), and is twice the average value of the fully extended cation (~15.5 Å), as calculated from the single crystal structure, which suggests interdigitation of the polyfluorinated chains, whose side-to-side separation accounts for the weak reflection at $q = 1.15\ Å^{-1}$.

An analogous lamellar organization of the LC state is also evident for $(MeImC_8H_4F_{13})_6Pb_3I_{12}$ (Figure 4b), whose high-temperature SAXS spectrum is dominated by a strong and sharp reflection at $q = 0.22\ Å^{-1}$ (periodicity of ca. 28.5 Å) as primary peak, similarly to the parent $MeImC_8H_4F_{13}I$ FILC (Figure S19b). A reduced periodicity is coherent with the shorter Im polyfluorinated chain of the latter perovskite-like material. Interestingly, while on cooling from the LC phase $(MeImC_9H_6F_{13})_6Pb_3I_{12}$ recovers its crystallinity (Figure 3a, Figure S16c, and Figure S19c), $(MeImC_8H_4F_{13})_6Pb_3I_{12}$ does not, supporting the formation of a vitrified SmA phase (Figure 3b, Figure S16d, and Figure S19d). This finding highlights that a slightly different

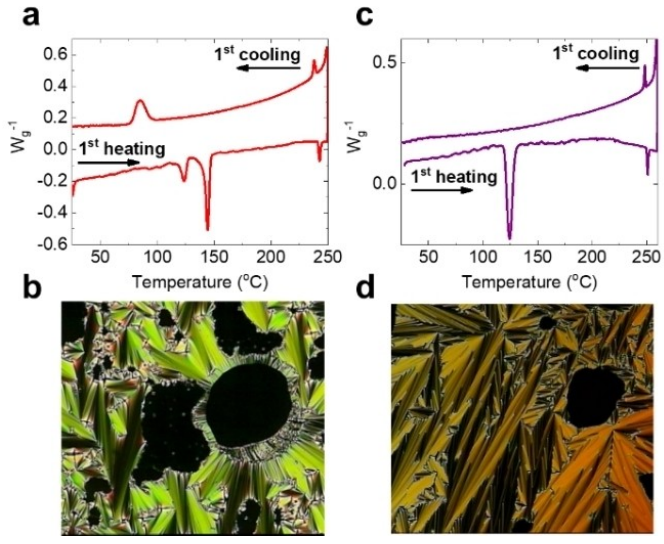

Figure 3. Differential Scanning Calorimetry (DSC) thermograms of: a) $(MeImC_9H_6F_{13})_6Pb_3I_{12}$ and c) $(MeImC_8H_4F_{13})_6Pb_3I_{12}$. Polarized Optical Microscope (POM) images of the liquid crystalline SmA phases of: b) $(MeImC_9H_6F_{13})_6Pb_3I_{12}$ at 160 °C and d) $(MeImC_8H_4F_{13})_6Pb_3I_{12}$ at 130 °C.

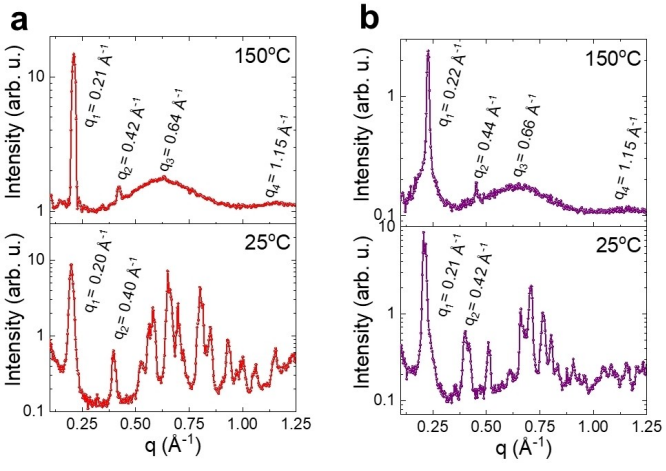

Figure 4. SAXS/WAXS spectra of a) $(MeImC_9H_6F_{13})_6Pb_3I_{12}$ and b) $(MeImC_8H_4F_{13})_6Pb_3I_{12}$ perovskite-like liquid crystals. For each system, the scattering profiles of the solid crystalline states (at 25 °C) and the high-temperature (150 °C) LC states, are presented.

molecular design may result in tailored structures and properties.

In summary, we have reported the synthesis and structural characterization of two novel liquid-crystalline hybrid organic–inorganic halides,[23a] i.e., perovskite-like materials, forming thermotropic smectic A mesophases. These new soft materials have been isolated by reacting lead iodide with two different fluorinated ionic liquid crystals (FILCs) based on imidazolium cations. The lamellar order of the new materials, both in the solid- and liquid-crystalline states, is directed by segregation and promoted by manifold intermolecular F···F interactions between the polyfluorinated chains of the imidazolium cations, serving as A-site cations. This leads to structural stabilization of the lead halide clusters, generating quasi-0D perovskite-like materials,[23b] which have been fully characterized, also from the optoelectronic properties point of view. Interestingly, a subtle change in the starting FILC resulted in the fine tuning of the thermal properties of the final perovskite mesophases, including vitrification of the fluid phase. The latter finding encourages further investigation on designing FILCs towards tailored liquid-crystalline perovskite-like soft materials for current application Schemes (i.e., defect passivation and interlayer engineering of photo/electro-active perovskite layers), as well as new ones, such as ferroelectricity. Furthermore, these results may also contribute to a deeper understanding of the chemistry and structure–property relationships in the booming field of metal halide perovskites, providing an outlook beyond the predominantly crystalline metal halide perovskite materials.

Supporting Information

Deposition Number 2266589 contains the supplementary crystallographic data for this paper. These data are provided free of charge by the joint Cambridge Crystallographic Data Centre and Fachinformationszentrum Karlsruhe Access Structures service www.ccdc.cam.ac.uk/structures.

Acknowledgements

We acknowledge Elettra Sincrotrone Trieste for providing access to its synchrotron radiation facilities (proposal number 20220569) and Maurizio Polentarutti and Giorgio Bais for assistance in using beamline X-RAY DIFFRACTION 1 (XRD1). PM acknowledges financial support from the project "Network 4 Energy Sustainable Transition — NEST", Spoke 4, Project code PE0000021, funded under the National Recovery and Resilience Plan (NRRP), Mission 4, Component 2, Investment 1.3 — Call for tender No. 1561 of 11.10.2022 of Ministero dell'Università e della Ricerca (MUR); funded by the European Union —NextGenerationEU. GT, PM, and GC acknowledge the financial support from the MUR, project SHINE (PRIN2022, no. 20225SYHXM). PM, GC, and AS acknowledge the financial support from the European Union's Horizon Europe research and innovation program, under the MSCA grant agreement No. 101059015, acronym HaloCell. SB acknowledges financial support from Horizon Europe EIC Pathfinder program, project 101098649 — UNICORN. The powder and small/wide angle X-ray diffraction experiments were carried out at the Next-GAME Laboratory of the Politecnico di Milano, co-funded by Regione Lombardia. Open Access publishing facilitated by Politecnico di Milano, as part of the Wiley - CRUI-CARE agreement.

Conflict of Interest

The authors declare no conflict of interest.

Data Availability Statement

The data that support the findings of this study are available in the supplementary material of this article.

Keywords: fluorous · crystal engineering · liquid crystal · perovskite · ionic liquid

[1] a) Y. Fu, H. Zhu, J. Chen, M. P. Hautzinger, X. Y. Zhu, S. Jin, *Nat. Rev. Mater.* **2019**, *4*, 169–188; b) J. Li, J. Duan, X. Yang, Y. Duan, P. Yang, Q. Tang, *Nano Energy* **2021**, *80*; c) X. Li, J. M. Hoffman, M. G. Kanatzidis, *Chem. Rev.* **2021**, *121*, 2230–2291; d) C. H. Liao, M. A. Mahmud, A. W. Y. Ho-Baillie, *Nanoscale* **2023**, *15*, 4219–4235.

[2] a) S. Sahare, H. D. Pham, D. Angmo, P. Ghoderao, J. MacLeod, S. B. Khan, S. L. Lee, S. P. Singh, P. Sonar, *Adv. Energy Mater.* **2021**, *11*, 2101085; b) J. Yan, T. J. Savenije, L. Mazzarella, O. Isabella, *Sustain. Energy Fuels* **2022**, *6*, 243–266; c) P. Metrangolo, L. Canil, A. Abate, G. Terraneo, G, Cavallo, *Angew. Chem. Int. Ed.* **2022**, *61*, e202114793.

[3] a) J. Chen, J. Wang, X. Xu, J. Li, J. Song, S. Lan, S. Liu, B. Cai, B. Han, J. T. Precht, D. Ginger, H. Zeng, *Nat. Photonics* **2020**, *15*, 238–244; b) Y. Tong, X. Bi, S. Xu, H. Min, L. Cheng, Z. Kuang, L. Yuan, F. Zhou, Y. Chu, L. Xu, L. Zhu, N. Zhao, N. Wang, W. Huang, J. Wang, *Adv. Mater.* **2023**, *35*, e2207111.

[4] a) Y. Wang, L. Song, Y. Chen, W. Huang, *ACS Photonics* **2019**, *7*, 10–28; b) H. P. Wang, S. Li, X. Liu, Z. Shi, X. Fang, J. H. He, *Adv. Mater.* **2021**, *33*, e2003309.

[5] a) S. P. Senanayak, M. Abdi-Jalebi, V. S. Kamboj, R. Carey, R. Shivanna, T. Tian, G. Schweicher, J. Wang, N. Giesbrecht, D. Di Nuzzo, H. E. Beere, P. Docampo, D. A. Ritchie, D. Fairen-Jimenez, R. H. Friend, H. Sirringhaus, *Sci. Adv.* **2020**, *6*, eaaz4948; b) J. Xia, X. Qiu, Y. Liu, P. A. Chen, J. Guo, H. Wei, J. Ding, H. Xie, Y. Lv, F. Li, W. Li, L. Liao, Y. Hu, *Adv. Sci.* **2023**, *10*, e2300133.

[6] Y. Rong, Y. Hu, A. Mei, H. Tan, M. I. Saidaminov, S. I. Seok, M. D. McGehee, E. H. Sargent, H. Han, *Science* **2018**, *361*.

[7] a) A. R. b. Mohd Yusoff, M. Vasilopoulou, D. G. Georgiadou, L. C. Palilis, A. Abate, M. K. Nazeeruddin, *Energy Environ. Sci.* **2021**, *14*, 2906–2953; b) C. Zhi, Z. Li, B. Wei, *APL Mater.* **2021**, *9*; c) L. Duan, A. Uddin, *Mater. Chem. Front.* **2022**, *6*, 400–417; d) X. Wu, B. Wu, Z. Zhu, M. Tayyab, D. Gao, *Solar RRL* **2022**, *6*.

[8] a) T. Niu, L. Chao, W. Gao, C. Ran, L. Song, Y. Chen, L. Fu, W. Huang, *ACS Energy Lett.* **2021**, 1453–1479; b) A. Liang, K. Wang, Y. Gao, B. P. Finkenauer, C. Zhu, L. Jin, L. Huang, L. Dou, *Angew. Chem. Int. Ed.* **2021**, *60*, 8337–8343; c) L. Chao,

T. Niu, Y. Xia, Y. Chen, W. Huang, *Acc. Mater. Res.* **2021**, *2*, 1059–1070; d) F. Fan, Y. Zhang, M. Hao, F. Xin, Z. Zhou, Y. Zhou, *J. Energy Chem.* **2022**, *68*, 797–810; e) J. Luo, F. Lin, J. Yuan, Z. Wan, C. Jia, *ACS Materials Lett.* **2022**, *4*, 1684–1715; f) H. Wu, Z. Li, F. Zhang, C. Kang, Y. Li, *Adv. Mater. Interfaces* **2022**, *9*.

[9] F. Wang, C.-y. Ge, D. Duan, H. Lin, L. Li, P. Naumov, H. Hu, *Small Structures* **2022**, *3*.

[10] a) S. Bai, P. Da, C. Li, Z. Wang, Z. Yuan, F. Fu, M. Kawecki, X. Liu, N. Sakai, J. T. Wang, S. Huettner, S. Buecheler, M. Fahlman, F. Gao, H. J. Snaith, *Nature* **2019**, *571*, 245–250; b) A. Wang, J. Wang, X. Niu, C. Zuo, F. Hao, L. Ding, *InfoMat* **2021**, *4*; c) X. Li, C. Li, X. Zhao, Y. Zhang, G. Liu, Z. Zhang, D. Wang, L. Xiao, Z. Chen, B. Qu, *ACS Appl. Mater. Interfaces* **2021**, *13*, 4553–4559; d) Y. Miao, Z. Wang, C. Chen, X. Ding, M. Zhai, L. Liu, Z. Xia, H. Wang, M. Cheng, *Solar RRL* **2022**, *6*; e) S.-H. Yang, C.-H. Tsai, X.-F. Wang, T.-C. Lee, C.-L. Liu, *Sustain. Energy Fuels* **2022**, *6*, 4962–4969.

[11] a) D. Yang, X. Zhou, R. Yang, Z. Yang, W. Yu, X. Wang, C. Li, S. Liu, R. P. H. Chang, *Energy Environ. Sci.* **2016**, *9*, 3071–3078; b) Q. Wu, W. Zhou, Q. Liu, P. Zhou, T. Chen, Y. Lu, Q. Qiao, S. Yang, *ACS Appl. Mater. Interfaces* **2016**, *8*, 34464–34473; c) D. Yang, R. Yang, X. Ren, X. Zhu, Z. Yang, C. Li, S. F. Liu, *Adv. Mater.* **2016**, *28*, 5206–5213; d) M. Li, C. Zhao, Z. K. Wang, C. C. Zhang, H. K. H. Lee, A. Pockett, J. Barbé, W. C. Tsoi, Y. G. Yang, M. J. Carnie, X. Y. Gao, W. X. Yang, J. R. Durrant, L. S. Liao, S. M. Jain, *Adv. Energy Mater.* **2018**, *8*; e) M. Salado, A. D. Jodlowski, C. Roldan-Carmona, G. de Miguel, S. Kazim, M. K. Nazeeruddin, S. Ahmad, *Nano Energy* **2018**, *50*, 220–228; f) N. K. Noel, S. N. Habisreutinger, B. Wenger, Y. H. Lin, F. Zhang, J. B. Patel, A. Kahn, M. B. Johnston, H. J. Snaith, *Adv. Energy Mater.* **2019**, *10*; g) J. Chen, X. Zhao, S. G. Kim, N. G. Park, *Adv. Mater.* **2019**, *31*, e1902902; h) W. Zhang, X. Liu, B. He, Z. Gong, J. Zhu, Y. Ding, H. Chen, Q. Tang, *ACS Appl. Mater. Interfaces* **2020**, *12*, 4540–4548; i) X. Zhu, M. Du, J. Feng, H. Wang, Z. Xu, L. Wang, S. Zuo, C. Wang, Z. Wang, C. Zhang, X. Ren, S. Priya, D. Yang, S. F. Liu, *Angew. Chem. Int. Ed.* **2021**, *60*, 4238–4244; j) F. Yu, Q. Han, L. Wang, S. Yang, X. Cai, C. Zhang, T. Ma, *Solar RRL* **2021**, *5*; k) X. Zhu, S. Yang, Y. Cao, L. Duan, M. Du, J. Feng, Y. Jiao, X. Jiang, Y. Sun, H. Wang, S. Zuo, Y. Liu, S. Liu, *Adv. Energy Mater.* **2021**, *12*; l) X. Pu, J. Han, S. Wang, H. Zhou, Q. Cao, J. Yang, Z. He, X. Li, *J. Mater.* **2021**, *7*, 1039–1048; m) R. Yin, K.-X. Wang, S. Cui, B.-B. Fan, J.-W. Liu, Y.-K. Gao, T.-T. You, P.-G. Yin, *ACS Appl. Energ. Mater.* **2021**, *4*, 9294–9303; n) J. H. Lee, B. Nketia-Yawson, J.-J. Lee, J. W. Jo, *Chem. Eng. J.* **2022**, *446*; o) X. Zhuang, X. Chen, L. Xu, S. Liu, Y. Wu, Z. Shi, Q. Zhou, B. Li, H. Yan, P. Reiss, H. Song, *J. Colloid Interface Sci.* **2022**, *622*, 469–480.

[12] S. Zhang, T. Xiao, F. Fadaei Tirani, R. Scopelliti, M. K. Nazeeruddin, D. Zhu, P. J. Dyson, Z. Fei, *Inorg. Chem.* **2022**, *61*, 5010–5016.

[13] a) T. Kato, J. Uchida, T. Ichikawa, T. Sakamoto, *Angew. Chem. Int. Ed.* **2018**, *57*, 4355–4371; b) J. Uchida, B. Soberats, M. Gupta, T. Kato, *Adv. Mater.* **2022**, *34*, e2109063.

[14] a) A. M. Giroud-Godquin, *Coord. Chem. Rev.* **1998**, *178–180*, 1485–1499; b) C. F. J. Faul, *Mol. Cryst. Liq. Cryst.* **2006**, *450*, 255–265; c) F. Camerel, F. Kinloch, O. Jeannin, M. Robin, S. K. Nayak, E. Jacques, K. A. Brylev, N. G. Naumov, Y. Molard, *Dalton Trans.* **2018**, *47*, 10884–10896.

[15] a) F. Guittard, E. Taffin de Givenchy, S. Geribaldi, A. Cambon, *J. Fluorine Chem.* **1999**, *100*, 85–96; b) C. Tschierske, *Top. Curr. Chem.* **2012**, *318*, 1–108; c) G. Cavallo, G. Terraneo, A. Monfredini, M. Saccone, A. Priimagi, T. Pilati, G. Resnati, P. Metrangolo, D. W. Bruce, *Angew. Chem. Int. Ed.* **2016**, *55*, 6300–6304; d) G. Cavallo, A. Abate, M. Rosati, G. Paolo Venuti, T. Pilati, G. Terraneo, G. Resnati, P. Metrangolo, *ChemPlusChem* **2021**, *86*, 469–474; e) C. Pigliacelli, A. Acocella, I. Diez, L. Moretti, V. Dichiarante, N. Demitri, H. Jiang, M. Maiuri, R. H. A. Ras, F. B. Bombelli, G. Cerullo, F. Zerbetto, P. Metrangolo, G. Terraneo, *Nat. Commun.* **2022**, *13*, 2607.

[16] A. Abate, A. Petrozza, G. Cavallo, G. Lanzani, F. Matteucci, D. W. Bruce, N. Houbenov, P. Metrangolo, G. Resnati, *J. Mater. Chem. A* **2013**, *1*, 6572–6578.

[17] V. M. Arivunithi, S. S. Reddy, V. G. Sree, H.-Y. Park, J. Park, Y.-C. Kang, E.-S. Shin, Y.-Y. Noh, M. Song, S.-H. Jin, *Adv. Energy Mater.* **2018**, *8*, 1801637–1801644.

[18] X. Xia, J. Peng, Q. Wan, X. Wang, Z. Fan, J. Zhao, F. Li, *ACS Appl. Mater. Interfaces* **2021**, *13*, 17677–17689.

[19] a) S. Kahmann, E. K. Tekelenburg, H. Duim, M. E. Kamminga, M. A. Loi, *Nat. Commun.* **2020**, *11*, 2344; b) E. K. Tekelenburg, S. Kahmann, M. E. Kamminga, G. R. Blake, M. A. Loi, *Adv. Opt. Mater.* **2021**, *9*; c) G. Li, Y. Zhang, W. Wang, L. Gao, Y. Ren, J. Che, C. Mo, H. Liu, W. Zhao, J. Lu, Z. Ni, *Adv. Opt. Mater.* **2022**, *10*; d) S. Kahmann, D. Meggiolaro, L. Gregori, E. K. Tekelenburg, M. Pitaro, S. D. Stranks, F. De Angelis, M. A. Loi, *ACS Energy Lett.* **2022**, *7*, 4232–4241.

[20] R. Pollice, P. Chen, *J. Am. Chem. Soc.* **2019**, *141*, 3489–3506.

[21] a) J. Kadam, C. F. J. Faul, U. Scherf, *Chem. Mater.* **2004**, *16*, 3867–3871; b) C. F. J. Faul, P. Krattiger, B. M. Smarsly, H. Wennemers, *J. Mater. Chem.* **2008**, *18*; c) M. T. Sims, L. C. Abbott, J. W. Goodby, J. N. Moore, *Soft Matter.* **2019**, *15*, 7722–7732; d) M. Ebert, I. Carrasco, N. Dumait, W. Frey, A. Baro, A. Zens, M. Lehmann, G. Taupier, S. Cordier, E. Jacques, Y. Molard, S. Laschat, *Chem. Eur. J.* **2022**, *28*, e202103446; e) P. Ehni, S. M. Bauch, P. M. Becker, W. Frey, A. Zens, J. Kastner, Y. Molard, S. Laschat, *Phys. Chem. Chem. Phys.* **2022**, *24*, 21617–21630.

[22] N. S. Elstone, K. Shimizu, E. V. Shaw, P. D. Lane, L. D′Andrea, B. Deme, N. Mahmoudi, S. E. Rogers, S. Youngs, M. L. Costen, K. G. McKendrick, J. N. Canongia Lopes, D. W. Bruce, J. M. Slattery, *J. Phys. Chem. B* **2023**, *127*, 7394–7407.

[23] a) Q. A. Akkerman, L. Manna, *ACS Energy Lett.* **2020**, *5*, 604–610; b) V. Trifiletti, C. Asker, G. Tseberlidis, S. Riva, K. Zhao, W. Tang, S. Binetti, O. Fenwick, *Front. Electron.* **2022**, *2*, 758603.

Manuscript received: May 6, 2024
Accepted manuscript online: June 24, 2024
Version of record online: August 7, 2024